Monthly Notices
of the
ROYAL ASTRONOMICAL SOCIETY

MNRAS **498,** 4901–4905 (2020) doi:10.1093/mnras/staa2703

# Investigating the multiband non-thermal emission of the 100 TeV source eHWC J2019+368 with a pulsar wind nebula scenario

Jun Fang [1,2]★ Lu Wen,[1] Huan Yu[3] and Songzhan Chen[2]

[1]*Department of Astronomy, Yunnan University, Kunming 650091, China*
[2]*Institute of High Energy Physics, Chinese Academy of Sciences, Beijing 100049, China*
[3]*Department of Physical Science and Technology, Kunming University, Kunming 650214, China*

Accepted 2020 September 2. Received 2020 September 2; in original form 2020 May 16

## ABSTRACT

eHWC J2019+368 is one of the sources emitting $\gamma$-rays with energies higher than 100 TeV based on the recent measurement with the High Altitude Water Cherenkov Observatory (HAWC), and the origin is still in debate. The pulsar PSR J2021+3651 is spatially coincident with the TeV source. We investigate theoretically whether the multiband non-thermal emission of eHWC J2019+368 can originate from the pulsar wind nebula (PWN) G75.2+0.1 powered by PSR J2021+3651. In the model, the spin-down power of the pulsar is transferred to high-energy particles and magnetic field in the nebula. As the particles with an energy distribution of either a broken power law or a power law continually injected into the nebula, the multiband non-thermal emission is produced via synchrotron radiation and inverse Compton scattering. The spectral energy distribution of the nebula from the model with the reasonable parameters is generally consistent with the detected radio, X-ray, and TeV $\gamma$-ray fluxes. Our study supports that the PWN has the ability to produce the TeV $\gamma$-rays of eHWC J2019+368, and the most energetic particles in the nebula have energies up to about 0.4 PeV.

**Key words:** radiation mechanisms: non-thermal – ISM: individual objects (G75.2+0.1).

## 1 INTRODUCTION

A source emitting $\gamma$-rays with energies above 100 TeV is a potential candidate which can accelerate cosmic rays to the 'knee' at ∼1 PeV. Detecting and identifying them can shed light on the primarily contributor to the Galactic cosmic rays. Recently, Abeysekara et al. (2020) reported that nine sources had been detected above 56 TeV with HAWC, and three of them, eHWC J1825-134, eHWC J1907+063, and eHWC J2019+368, emit $\gamma$-rays past 100 TeV.

The 100 TeV source eHWC J2019+368 has an integral flux of $\sim 1.6 \times 10^{-14}$ ph cm$^{-2}$ s$^{-1}$ above 56 TeV based on the HAWC results (Abeysekara et al. 2020). It is within the Cygnus region, which is composed of some potential cosmic ray accelerators (Abdo et al. 2007a; Bi et al. 2009; Bartoli et al. 2012; Abeysekara et al. 2018). This source was first detected with Milagro (MGRO J2019+37) in TeV $\gamma$-rays with a flux of ∼ 80 per cent of the Crab nebula (Abdo et al. 2012). Moreover, the observation with VERITAS indicated an extended source VER J2016+378 constitutes the bulk of the TeV emission, and the $\gamma$-ray region contains the energetic pulsar PSR J2021+3651 and the star formation region Sh 2-104 (Aliu et al. 2014).

GeV $\gamma$-rays from PSR J2021+3651 have been detected with *Fermi*-LAT, and the upper limit on the GeV $\gamma$-rays from the putative PWN named G75.2+0.1 (Hessels et al. 2004; Van Etten, Romani & Ng 2008), is < 10 per cent of the pulsed emission (Abdo et al. 2009). Mizuno et al. (2017) performed X-ray studies on VER J2016+378 using the data of *Suzaku* and *XMM–Newton*. The X-ray nebula was indicated to have an extension of more than 27 arcmin along the major axis, and the association of it with the TeV source VER J2016+378 was supported. Based on the multiband data obtained with *XMM–Newton*, *INTEGRAL*, and *Fermi*-LAT, Hou et al. (2014) proposed that the $\gamma$-rays of MGRO J2019+37 might be produced by the high-energy electrons in G75.2+0.1.

Terminate shocks in PWNe are generated due to the interaction of the relativistic winds blown from the pulsars with the ambient medium, and the energy of the flow can be efficiently transferred into electrons/positrons and magnetic field (Gaensler & Slane 2006; Amato 2020). Particle in cell simulations on relativistic shocks indicated that the electrons/positrons could be accelerated to high-energies when they bounce around the shock (Spitkovsky 2008; Crumley et al. 2019). Studies on PWNe indicated that they had the ability to produce multiwavelength non-thermal emission from radio to TeV $\gamma$-rays via synchrotron radiation and inverse Compton scattering.

In this paper, we investigate whether the nebula G75.2+0.1 powered by the pulsar PSR J2021+3651 has the ability to produce the TeV flux of eHWC J2019+368 with appropriate parameters based on a time-dependent model for the multiband non-thermal emission from PWNe. In Section 2, the detail of the model is described. The results on the nebula are presented in Section 3. Finally, the discussion and summary are given in Section 4.

## 2 THE MODEL FOR THE MULTIBAND NON-THERMAL EMISSION FROM PWNE

In a PWN, high-energy leptons (electrons and positrons) are continually injected when the pulsar spins down gradually. The lepton distribution $N(\gamma, t)$ at time $t$ can be solved from the diffusion equation

★ E-mail: fangjun@ynu.edu.cn

(e.g. Fang & Zhang 2010; Martín, Torres & Rea 2012)

$$\frac{\partial N(\gamma,t)}{\partial t}=\frac{\partial}{\partial\gamma}[\dot{\gamma}(\gamma,t)N(\gamma,t)]-\frac{N(\gamma,t)}{\tau(\gamma,t)}+Q(\gamma,t)\,, \tag{1}$$

where $\dot{\gamma}(\gamma,t)$ is the energy loss rate of the Lorentz factor of the leptons, $\tau(\gamma,t)$ is the escape time due to Bohm diffusion (Zhang, Chen & Fang 2008), and $Q(\gamma,t)$ represents the injection of the particles per unit time in the whole nebula.

For a pulsar with period $P$, period-derivative $\dot{P}$, breaking index $n$ and age $t_{\rm age}$, the characteristic age is $\tau_c=P/2\dot{P}$, and the spin-down luminosity is

$$L(t)=4\pi^2 I\frac{P}{\dot{P}^3}, \tag{2}$$

where the moment of inertia of the pulsar $I$ is adopted to be $10^{45}\,{\rm g\,cm^2}$ in this paper. The injection luminosity equals $L(t)$, and it follows (Gaensler & Slane 2006)

$$L(t)=L_0\left(1+\frac{t}{\tau_0}\right)^{-\frac{n+1}{n-1}}, \tag{3}$$

where $L_0$ is the initial luminosity, and the initial spin-down time-scale of the pulsar is

$$\tau_0=\frac{2\tau_c}{n-1}-t_{\rm age}. \tag{4}$$

The spin-down luminosity is transferred into particles and magnetic field. Assuming the magnetic energy fraction is $\eta$, the magnetic field strength in the PWN is (Tanaka & Takahara 2010; Martín et al. 2012)

$$B(t)=\frac{3(n-1)\eta L_0\tau_0}{R^3_{\rm PWN}(t)}\left[1-\left(1+\frac{t}{\tau_0}\right)^{\frac{2}{n-1}}\right], \tag{5}$$

and the radius of the nebula in the free expanding phase is (van der Swaluw et al. 2001, 2003; Torres et al. 2014)

$$R_{\rm PWN}(t)=0.84\left(\frac{L_0t}{E_0}\right)^{1/5}\left(\frac{10E_0}{3M_{\rm ej}}\right)^{1/2}t, \tag{6}$$

where $E_0=10^{51}\,{\rm erg}$ is the kinetic energy of the supernova ejecta with a mass of $M_{\rm ej}=9.5\,{\rm M}_\odot$ for the PWN in this paper. $\eta=0.03$ is adopt in Torres et al. (2014) to model the Crab nebula, and we also use this fraction in this paper.

Leptons are continually injected into the PWN with a distribution of a power law (Kennel & Coroniti 1984; Reynolds & Chevalier 1984)

$$Q(\gamma,t)=Q_0(t)\gamma^{-\alpha}, \tag{7}$$

or a broken power law (Kennel & Coroniti 1984; Reynolds & Chevalier 1984)

$$Q(\gamma,t)=Q_0(t)\begin{cases}\left(\frac{\gamma}{\gamma_{\rm b}}\right)^{-\alpha_1} & \text{if } \gamma\le\gamma_{\rm b}\,,\\ \left(\frac{\gamma}{\gamma_{\rm b}}\right)^{-\alpha_2} & \text{if } \gamma_{\rm b}<\gamma\le\gamma_{\rm max}\,.\end{cases} \tag{8}$$

$Q_0(t)$ is given by (Martín et al. 2012; Torres et al. 2014)

$$(1-\eta)L(t)=\int\gamma m_{\rm e}c^2Q(\gamma,t){\rm d}\gamma. \tag{9}$$

The maximum energy of the particles is determined according to the Larmor radius $R_{\rm L}$ must be smaller than a fraction of the radius of the termination shock $R_{\rm s}$, i.e. $R_{\rm L}=\varepsilon R_{\rm s}$, where $\varepsilon$ is the fractional size of the shock (Martín et al. 2012). A range of $0.2\le\varepsilon\le1/3$ is usually adopted to derive the maximum energy of the particles for PWNe

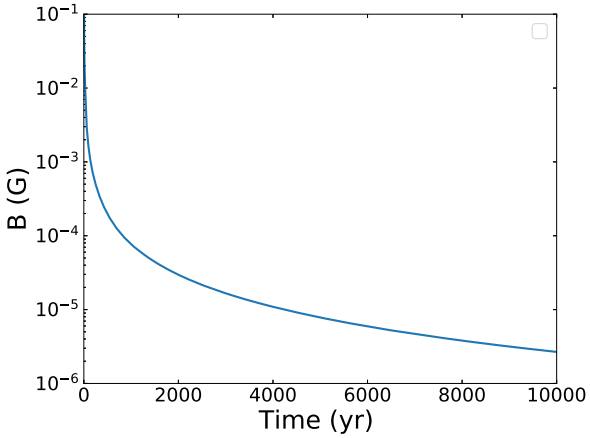


**Figure 1.** The evolution of the magnetic field strength in the PWN with $\eta=0.03$.

(Martín et al. 2012; Torres et al. 2014). The maximum Lorentz factor can be derived from (Martín et al. 2012; Torres et al. 2014)

$$\gamma_{\rm max}(t)=\frac{\varepsilon e\kappa}{m_{\rm e}c^2}\left(\frac{\eta L(t)}{c}\right)^{1/2}, \tag{10}$$

where $m_{\rm e}$, $e$ are the electron mass and charge. For strong shocks, the magnetic compression ratio at the shock is about 3, and we fix $\kappa$ to 3 in this paper (Holler et al. 2012; Martín et al. 2012).

After the particles are injected into the PWN, they encounter adiabatic and radiation losses. Multiband non-thermal emission is produced via synchrotron and inverse Compton scattering off the background soft photons, which consist of the synchrotron emission, cosmic-microwave background (CMB), and IR/optical photon fields. Details of the formulae on the two radiative processes used in the calculation can be found in the appendixes of Martín et al. (2012).

## 3 RESULTS

The rotational period of the pulsar PSR J2021+3651 is $0.104\times10^{-3}$ s (Roberts et al. 2002). With the first period derivative $\dot{P}=9.6\times10^{-14}\,{\rm s\,s^{-1}}$ , the characteristic age is $\tau_{\rm c}=1.7\times10^4$ yr, and the current luminosity is $3.4\times10^{36}\,{\rm erg\,s^{-1}}$. The distance of the pulsar has been estimated to be $1.8^{+1.7}_{-1.4}$ kpc (Kirichenko et al. 2015), and we adopt 1.8 kpc in this paper. The three interstellar photon fields involved in calculating the spectrum of the inverse Compton scattering are CMB with temperature $T_{\rm cmb}=2.7\,{\rm K}$ and energy density $U_{\rm cmb}=0.25\,{\rm eV\,cm^{-3}}$, IR background with $T_{\rm IR}=30\,{\rm K}$ and $U_{\rm IR}=0.3\,{\rm eV\,cm^{-3}}$ (Mizuno et al. 2017), and star light (SL) with $T_{\rm s}=5000\,{\rm K}$ and $U_{\rm s}=1\,{\rm eV\,cm^{-3}}$.

The age of PSR J2021+3651 is unknown, and we first adopt it to be $10^4$ yr. With this age, the initial spin-down time-scale is $\tau_0=7.15\times10^3$ yr, and the initial luminosity is $L_0=1.95\times10^{37}\,{\rm erg\,s^{-1}}$. Torres et al. (2014) investigated the multiband radiative properties of some TeV-detected PWNe, the energies contained in the particles and the magnetic field do not satisfy equipartition. The magnetic energy ratio $\eta$ is usually <0.1 to reproduce the detected multiband fluxes for the PWNe. As illustrated in Fig. 1 and equation (5), the magnetic field decreases with time due to the expansion of the nebula. With $\eta=0.03$, which is the same as the Crab nebula in Torres et al. (2014), the magnetic field strength in the nebula is 2.7 μG at a time of $10^4$ yr. Fig. 2 indicates the cooling times for the synchrotron radiation, the adiabatic loss, the inverse Compton scattering, and the escape time due to the Bohm diffusion for the particles with different Lorentz

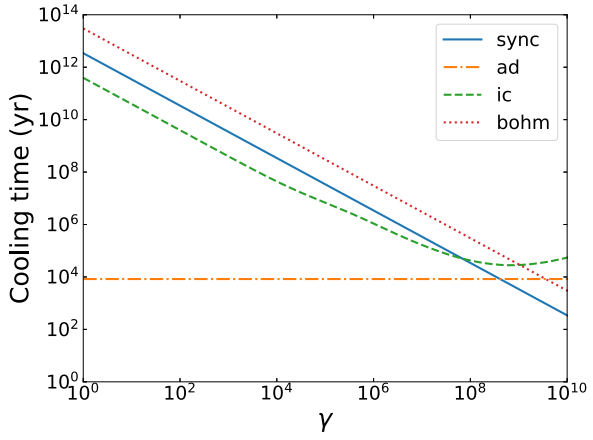


**Figure 2.** Cooling times for synchrotron radiation, adiabatic loss, inverse Compton scattering, and the escape time for Bohm diffusion at $t_{age} = 10^4$ yr.

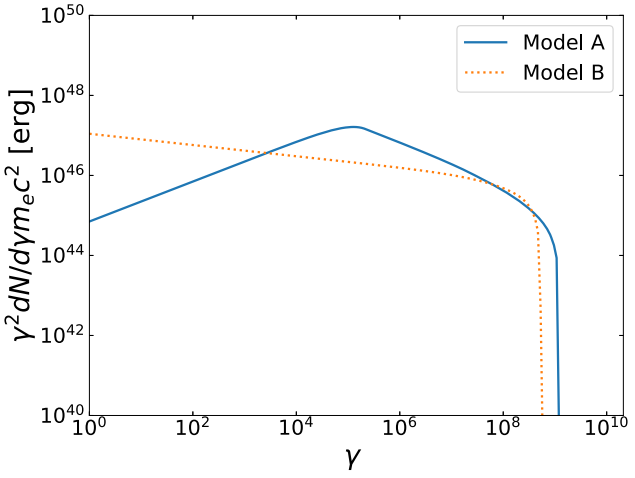


**Figure 3.** Particle distributions of the electrons/positrons in the nebula on $\gamma$ for the models A and B at $t_{age} = 10^4$ yr.

factor. For $\gamma < 10^8$, the adiabatic loss is the dominate process to cool the particles. For $5 \times 10^8 < \gamma < 5 \times 10^9$, the synchrotron radiation becomes the most prominent process, and the particles with $\gamma \sim 10^{10}$ escape quickly from the nebula via the Bohm diffusion.

With the assumption that the particles injected in G75.2+0.1 have a broken power-law distribution with $\alpha_1 = 1.5$, $\alpha_2 = 2.5$, $\gamma_b = 2.0 \times 10^5$, and $\varepsilon = 1/3$ (model A). At $t_{age} = 10^4$ yr, as indicated in Fig. 3, the particle spectrum has a break at $\gamma_b$ and a cut-off Lorentz factor $\sim 1.2 \times 10^9$ ($\sim$0.6 PeV). The resulting photon spectra at $t_{age} = 10^4$ yr from the synchrotron, the SSC and the inverse Compton scattering off the CMB, IR background and SL are illustrated in Fig. 4. The radio flux density detected with the Very Large Array (VLA) is 700 mJy at 1.4 GHz for the extended emission with an extension of $\sim$100 arcmin$^2$ in the vicinity of the PWN G75.2+0.1 (Paredes et al. 2009). The X-ray spectrum derived from the observations with *Suzaku* and *XMM–Newton* corresponds to a flux of $7 \times 10^{-12}$ erg cm$^{-2}$ s$^{-1}$ with a photon index of 2.05 in 2–10 keV for the overall PWN (Mizuno et al. 2017). The fluxes with VERITAS for the source VER J2019+368 and Milagro for MGRO J2019+37 at 12, 20, 35 TeV are also shown in Fig. 4. The spectrum of VER J2019+378 detected by VERITAS can be fitted with a power law with an index of $\sim$1.75 in 1–10 TeV (Aliu et al. 2014) and the

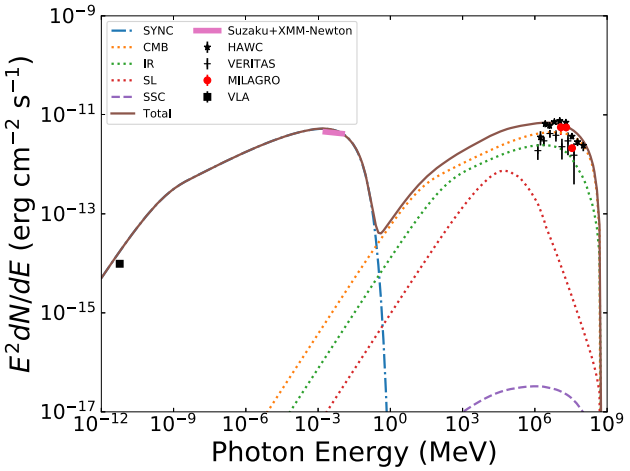


**Figure 4.** Spectral energy distribution from the model for the PWN G75.2+0.1 with $t_{age} = 10^4$ yr. The observed fluxes in the radio, X-ray and $\gamma$-ray bands are taken from Paredes et al. (2009), Mizuno et al. (2017), Abdo et al. (2007a,b, 2009a), Aliu et al. (2014), and Abeysekara et al. (2020).

detected $\gamma$-ray flux is lower than that with HAWC. The observational results are summarized in Table 1. The synchrotron spectrum has a break at $\sim 10^{-9}$ MeV due to the change of the index of the particle spectrum at $\gamma_b$, and the higher energy cutoff at several keV results from the energy losses. In the TeV band, the $\gamma$-rays are mainly produced via the inverse Compton scattering off the CMB and IR photons, and the SSC process is negligible in producing the $\gamma$-rays with such a low magnetic field strength of 2.7 μG. The resulting spectrum from the inverse Compton scattering is consistent with those obtained by HAWC with energies above 3 TeV, but at lower energies the $\gamma$-ray flux from the model is significantly higher than those by either HAWC or VERITAS.

With an age of $10^4$ yr, the spectral energy distributions at different times are indicated in Fig. 5. The synchrotron radiation diminishes significantly with time because the magnetic field decreases due to the expansion of the nebula. In the $\gamma$-ray band above 10 MeV, the spectrum from the inverse Compton scattering after a time of $\sim 10^4$ yr saturates due to the balance of the injection of the high-energy particles and the processes of the energy losses.

The effect of the age on the resulting multiband spectral energy distribution of the PWN is illustrated in Figs 6 and 7. With an age of $8 \times 10^3$ yr, the initial luminosity is $L_0 = 1.2 \times 10^{37}$erg s$^{-1}$, and less energy is injected in the nebula compared with $t_{age} = 10^4$ yr. As illustrated in Fig. 6, the resulting flux in the band of 1–30 TeV is lower than that obtained with HAWC. Whereas for $t_{age} = 1.2 \times 10^4$ yr, a higher initial luminosity $L_0 = 3.8 \times 10^{37}$erg s$^{-1}$ is adopted, and the resulting $\gamma$-ray flux is relatively higher than the HAWC result (see Fig. 7). Therefore, with the energy densities of the background radiation field and the broken power-law spectrum for the high-energy particles used in the model, an age of $10^4$ yr is preferred to reproduce the detected TeV $\gamma$-ray flux with HAWC.

Fig. 8 indicates the resulting multiband spectrum assuming the particle injected into the nebula has a distribution of a power law with $\alpha = 2.14$ and $t_{age} = 10^4$ yr (model B). The maximum energy of the particles in the nebula and that of the most energetic $\gamma$-rays depend sensitively on $\varepsilon$, which is constrained to 0.15 to reproduce the spectrum in the TeV $\gamma$-rays measured with HAWC. The leptons have a power-law distribution on the Lorentz factor with a cut-off energy of $\sim$0.4 PeV (Fig. 3), and the break of the resulting spectrum for the synchrotron at $\sim 10^{-9}$ MeV disappears. The resulting flux in

**Table 1.** Summary of observations.

| Observatory | $E^2$d$N$/d$E$ erg cm$^{-2}$ s$^{-1}$ | Energy (range) MeV | Source name (extension) | Reference |
|---|---|---|---|---|
| VLA | $5.8 \times 10^{-12}$ | $9.8 \times 10^{-15}$ | (∼100 arcmin$^2$) | Paredes et al. (2009) |
| *Suzaku, XMM–Newton* | $7 \times 10^{-12}$ | (2–10) $\times 10^{-3}$ | (∼30 arcmin × 12 arcmin) | Mizuno et al. (2017) |
| VERITAS | | (1–30) $\times 10^{6}$ | VER J2019+368 (∼20.4 arcmin × 7.8 arcmin) | Aliu et al. (2014) |
| HAWC | | (1–177) $\times 10^{6}$ | eHWC J2019+368 (0.20 ± 0.05°) | Abeysekara et al. (2020) |
| Milagro | $(5.6 \pm 1.7) \times 10^{-12}$ | $12 \times 10^{6}$ | MGRO J2019+37 | Abdo et al. (2007a) |
| | $(5.6 \pm 0.9) \times 10^{-12}$ | $20 \times 10^{6}$ | MGRO J2019+37 (1.1 ± 0.5°) | Abdo et al. (2007b) |
| | $(2.1 \pm 0.2) \times 10^{-12}$ | $35 \times 10^{6}$ | MGRO J2019+37 | Abdo et al. (2009a) |

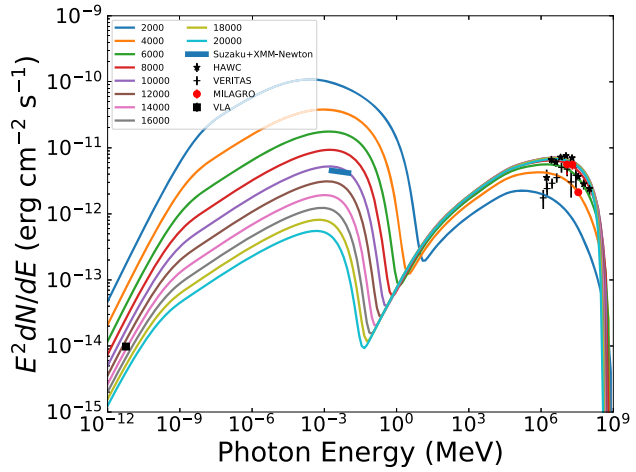


**Figure 5.** The spectral energy distributions at different times from the model for the PWN G75.2+0.1 with $t_{age} = 10^4$ yr. The others are the same as Fig. 4.

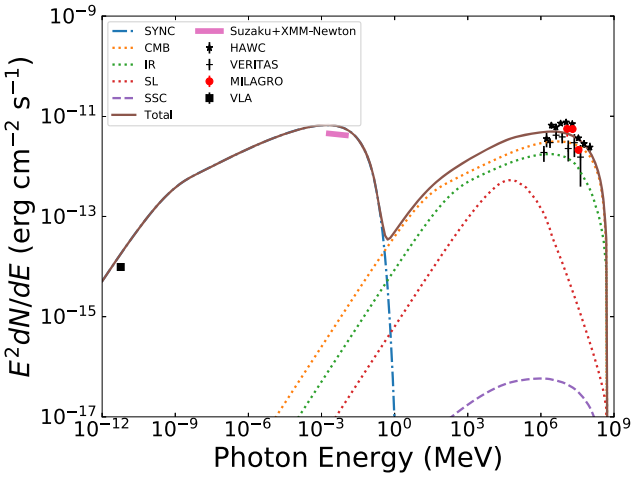


**Figure 6.** Spectral energy distribution from the model for G75.2+0.1 with $t_{age} = 8 \times 10^3$ yr. The others are the same as Fig. 4.

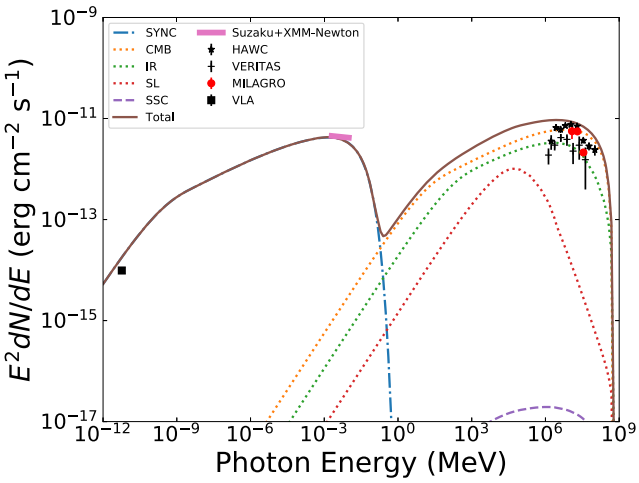


**Figure 7.** Spectral energy distribution from the model for G75.2+0.1 with $t_{age} = 1.2 \times 10^4$ yr. The others are the same as Fig. 4.

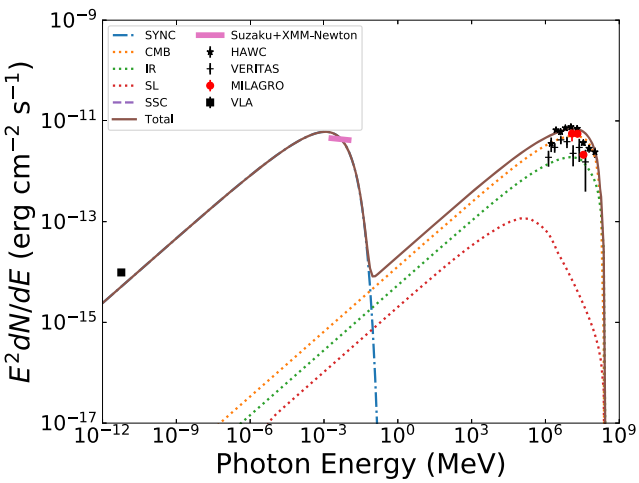


**Figure 8.** Spectral energy distribution from the model for G75.2+0.1 with $t_{age} = 1.0 \times 10^4$ yr and a power-law spectrum of the injected particles ($\alpha = 2.14$). The others are the same as Fig. 4.

the band 1–10 TeV is significantly lower than that with the broken power-law distribution for the injected particles in the model A. The flux in 3–20 TeV is consistent well with that detected by HAWC, and the slope of the spectrum in 1–10 TeV obtained by VERITAS can be better reproduced than the model A. The multiband spectral energy distribution depends sensitively on the index of the power-law distribution for the particles. Fig. 9 shows the spectral energy distribution for the nebula with $\alpha = 2.1$ and the other parameters same as the model B. With such a harder spectrum, the fluxes both in the X-rays and in the $\gamma$-rays are higher than the detected ones.

## 4 SUMMARY AND DISCUSSION

We study the multiband non-thermal emission of the PWN G75.2+0.1 based on the time-dependent model, and investigate

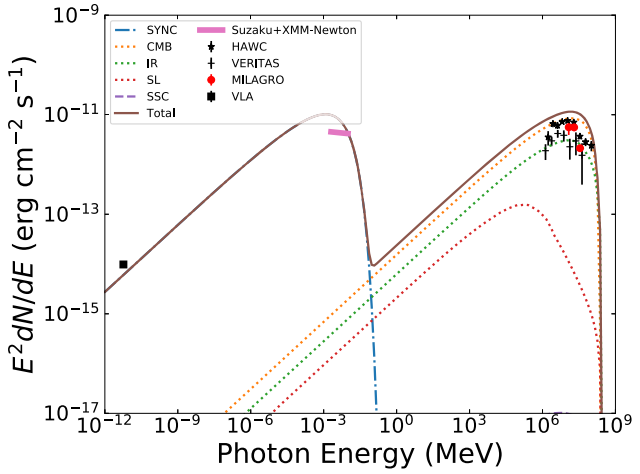


**Figure 9.** Spectral energy distribution from the model for G75.2+0.1 with a power-law spectrum of the injected particles ($\alpha = 2.1$). The others are the same as Fig. 8.

whether the nebula has the ability to produce the TeV $\gamma$-rays of eHWC J2019+368. Assuming the electrons/positrons injected into the nebula has the broken power-law distribution, the resulting spectral energy distribution of the PWN is generally consistent with the fluxes detected by VLA, *Suzaku* + *XMM–Newton* and HAWC except at 1.7 TeV. With the power-law spectrum for the injected particles in the model B, the $\gamma$-ray flux at 1.7 TeV detected by HAWC and the slope of the spectrum in the band 1–10 TeV obtained by VERITAS can be better reproduced than the model A. Our studies indicate that the PWN G75.2+0.1 powered by the energetic pulsar PSR J2021+3651 is capable of producing the $\gamma$-ray flux of eHWC J2019+368 with the reasonable parameters, and the energetic electrons/positrons in the nebula have energies up to ∼0.4 PeV.

The $\gamma$-ray flux resulting from the inverse Compton scattering depends on the age of the pulsar, because more energy can be injected into the high-energy electrons/positrons in the nebula with an older age. Since the injection of the high-energy particles is balanced by the energy losses after a certain time, the TeV $\gamma$-rays resulting from the inverse Compton scattering saturates. With $\eta = 0.03$, an age of $10^4$ yr is derived in this paper to reproduce a $\gamma$-ray flux consistent with the measurements in the TeV band. However, the preferred age depends sensitively on the distance of the pulsar. A larger distance implies an older age of the pulsar to reproduce the detected $\gamma$-ray flux in the TeV band.

The Crab nebula is also a $\gamma$-ray source emitting photons with energies past 100 TeV. Assuming the particles injected into the nebula have a spectrum of a broken power law with $\alpha_1 = 1.5$, $\alpha_2 = 2.5$, and $\gamma_b = 7 \times 10^5$, the multiband spectrum consists well with the observed fluxes from radio to $\gamma$-rays (Torres et al. 2014). The two indexes are the same as those used in the model A of this paper for the PWN powered by PSR J2021+3651. The initial luminosity of the Crab pulsar is $\sim 3.1 \times 10^{39}$erg s$^{-1}$ (Torres et al. 2014), which is about 16 times higher than that PSR J2021+3651 in this paper. However, the inferred age for PSR J2021+3651 is about 10 times older than the Crab pulsar, and the spin-down energy has been injected into the nebula for a longer time compared with the Crab nebula. As a result, G75.2+0.1 has the comparable ability to produce $\gamma$-rays as the Crab nebula.

Some of the detected TeV $\gamma$-rays of eHWC J2019+368 may be originated from the other sources in the Cygnus region besides G75.2+0.1, such as the particles accelerated from the ensemble of OB associations (Hou et al. 2014) and the H II region Sh 2-104 (Aliu et al. 2014). Further observations with the Large High Altitude Air Shower Observatory (LHAASO) will give more insights into the origin the high-energy particles producing the TeV $\gamma$-rays of eHWC J2019+368 (Bai et al. 2019).

## ACKNOWLEDGEMENTS

We would like to thank the anonymous referee for very helpful comments to improve the paper. JF is partially supported by the Natural Science Foundation of China (NSFC) under grant no. 11873042, the applied basic research program of Yunnan Province under (2018FY001(-003)), the Candidate Talents Training Fund of Yunnan Province (2017HB003), the National Key R&D Program of China under grant no. 2018YFA0404204, and the Program for Excellent Young Talents, Yunnan University (WX069051, 2017YDYQ01).

## DATA AVAILABILITY

The data underlying this paper will be shared on reasonable request to the corresponding author.

## REFERENCES

Abdo A. A. et al., 2007a, ApJ, 658, L33
Abdo A. A. et al., 2007b, ApJ, 664, L91
Abdo A. A. et al., 2009a, ApJ, 700, L127
Abdo A. A. et al., 2009b, ApJ, 700, 1059
Abdo A. A. et al., 2012, ApJ, 753, 159
Abeysekara A. U. et al., 2018, ApJ, 861, 134
Abeysekara A. U. et al., 2020, Phys. Rev. Lett., 124, 021102
Aliu E. et al., 2014, ApJ, 788, 78
Amato E., 2020, preprint (arXiv:2001.04442)
Bai X. et al., 2019, preprint (arXiv:1905.02773)
Bartoli B. et al., 2012, ApJ, 745, L22
Bi X.-J., Chen T.-L., Wang Y., Yuan Q., 2009, ApJ, 695, 883
Crumley P., Caprioli D., Markoff S., Spitkovsky A., 2009, MNRAS, 485, 5105
Fang J., Zhang L., 2010, A&A, 525, A20
Gaensler B. M., Slane P. O., 2006, ARA&A, 44, 17
Hessels J. W. T., Roberts M. S. E., Ransom S. M., Kaspi V. M., Romani R. W., Ng C. -Y., Freire P. C. C., Gaensler B. M., 2004, ApJ, 612, 389
Holler M. et al., 2012, A&A, 539, A24
Hou C., Chen S.-Z., Yuan Q., Cao Z., Hui-Hai H., Sheng X.-D., 2014, Chin. Phys. C, 38, 085001
Kennel C. F., Coroniti F. V., 1984, ApJ, 283, 710
Kirichenko A. et al., 2015, ApJ, 802, 17
Martín J., Torres D. F., Rea N., 2012, MNRAS, 427, 415
Mizuno T. et al., 2017, ApJ, 841, 104
Paredes J. M. et al., 2009, A&A, 507, 241
Reynolds S. P., Chevalier R. A., 1984, ApJ, 278, 630
Roberts M. S. E., Hessels J. W. T., Ransom S. M., Kaspi V. M., Freire P. C. C., Crawford F., Lorimer D. R., 2002, ApJ, 577, L19
Spitkovsky A., 2008, ApJ, 682, L5
Tanaka S. J., Takahara F., 2010, ApJ, 715, 1248
Torres D. F., Cillis A., Martín J., de Oña Wilhelmi E., 2014, J. High Energy Astrophys., 1, 31
van der Swaluw E., 2003, A&A, 404, 309
van der Swaluw E., Achterberg A., Gallant Y. A., Tóth G., 2001, A&A, 380, 309
Van Etten A., Romani R. W., Ng C.-Y., 2008, ApJ, 680, 1417
Zhang L., Chen S. B., Fang J., 2008, ApJ, 676, 1210

This paper has been typeset from a TEX/LATEX file prepared by the author.